Device physics of polymer:fullerene bulk heterojunction solar cells

Bartesaghi, Davide

CHAPTER 1

INTRODUCTION TO ORGANIC SOLAR CELLS

Summary

The increasing need for energy can be satisfied by harvesting energy directly from sunlight; organic photovoltaics offer the possibility to do so in a cheap and sustainable way. This chapter is an introduction to organic photovoltaics, with an overview of the basic device physics. After discussing the experimental and simulation techniques which were used for this work, an outline of the thesis is given.

1.1 Solar energy

Among the problems that modern day society is facing, the increasing need for energy is certainly one of the most pressing. During all the industrial age, the production* of energy has largely relied on the use of fossil fuels. Besides the environmental pollution that is caused by burning fossil fuels, an important problem is that these sources of energy are non-renewable: by the end of this century, most of the fossil fuels will have run out.[1] It is therefore necessary to radically change our energy production, switching to renewable sources such as solar, wind and nuclear, which nowadays provides around 2%[2] of the total energy produced worldwide.

The world energy consumption per year amounted to 5.598 x 10^{20} J in 2012,[3] and it is constantly increasing. Although this amount of energy seems enormous, it is just a small fraction of the energy that every year reaches the Earth from the Sun, approximately 3.85 x 10^{24} J. Efficiently harvesting solar energy would meet all our needs for energy practically forever, as the Sun will continue to burn for the next 5 billion years.

State-of-the-art technologies for harvesting solar energy are based on inorganic semiconductors and have a record power conversion efficiency beyond 45%[4], although the efficiency of the commercially available solar cells for terrestrial use is around 20%. A drawback of these technologies is the higher price if compared to the non-renewable sources.

Organic photovoltaics (OPV) represent a valid alternative to the use of inorganic-based modules, because of the potential for relative low-cost and ease of devices fabrication,[5] the possibility of producing flexible and light devices,[6,7] and the environmental sustainability.[8,9] Using organic thin films, power conversion efficiencies above 10% have been achieved both in single layer and in tandem architecture.[10,11] Aiming at the commercialization of OPV technologies capable to compete with conventional inorganic solar cells, both the efficiency and the stability of OPV devices need to be improved. This requires a thorough understanding of the fundamental processes that occurs in the OPV devices.

1.2 Solar cell efficiency

Figure 1.1 represents a typical current-voltage (JV) curve of a solar cell under illumination. The current density at zero bias is called short-circuit current (J_{sc}); the applied bias at which the current density is zero is the open-circuit voltage (V_{oc}). The power generated by the cell is given by the product of J and V in the fourth quadrant of the plot. Its maximum value is reached at the maximum power point (MPP), at which the applied bias is V_{max} and the corresponding current density is J_{max}. It is customary in the field of photovoltaics to define the fill-factor FF as

*The terms "production" and "consumption" referred to energy are not physically correct. It is however common language to use them, and so do I in the first paragraph of this thesis.

$$FF = \frac{J_{max} V_{max}}{J_{sc} V_{oc}}. \tag{1.1}$$

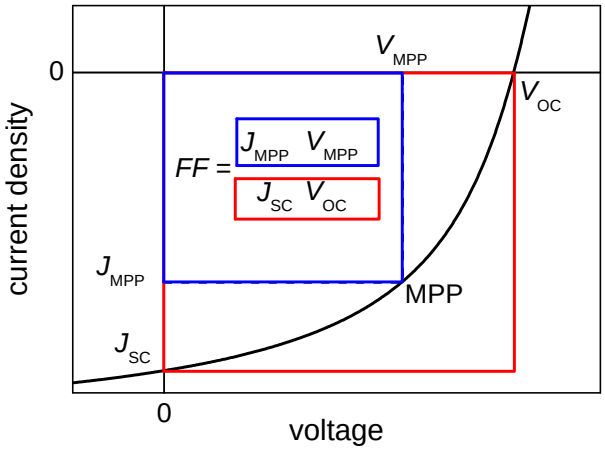

Figure 1.1: Current-voltage characteristic of a solar cell under illumination.

The power conversion efficiency (PCE) of the solar cell can be calculated using J_{sc}, V_{oc} and FF, according to

$$PCE = \frac{J_{sc} V_{oc} FF}{I}, \tag{1.2}$$

where I is the incident light intensity. The power conversion efficiency has to be determined under standard test conditions (STC), which include the temperature of the cell (25 °C), the light intensity (1 Sun, equal to 1000 W/m^2) and the spectral distribution of the light (air mass 1.5)*.

1.3 Organic semiconductors

Electrical conductivity in organic materials has been proved in the 1950s;[12,13] since then, the research field of organic electronic has gone trough a rapid development. A milestone paper was written 1977 by Shirakawa, MacDiarmid and Heeger.[14] Their work, for which they were awarded of the Nobel prize in chemistry in 2000, demonstrated the possibility of controlling the conductivity of conjugated polymers by doping. Conjugated polymers have been used successfully to fabricate organic light emitting

*The air mass 1.5, or AM1.5, is the spectrum of sunlight after passing through 1.5 times the thickness of Earth's atmosphere

diodes (OLEDs)[15] and solar cells.[16] The field is however not limited to conjugated polymers, and devices have been realized also with conducting small molecules.[17,18]

Whether they are polymers or small molecules, all organic semiconductors owe their electrical properties to conjugated π-electrons. A conjugated organic system is made by an alternation of single and double covalent bonds between carbon atoms (Figure 1.2). Single bonds are always strong σ-bonds, in which the two bonding electrons are localized in the region between the nuclei of the two atoms that share them. Double bonds contains a σ-bond and a weaker π-bond, in which electrons are more mobile. The wave functions of π-electrons are delocalized and extend beyond the two atoms.

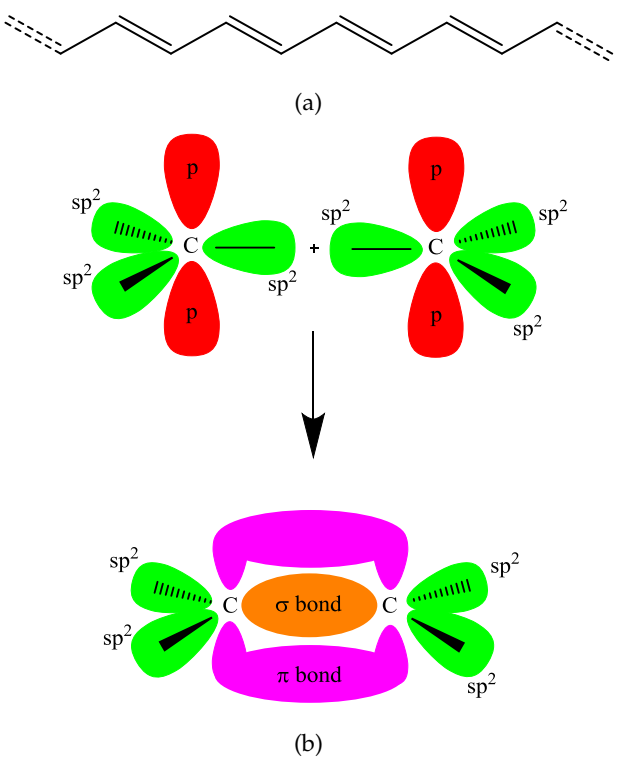

Figure 1.2: a) Chemical structures of polyacetylene, the simplest conjugated polymer; b) schematic image of the formation of a double bond between two carbon atoms. The overlap of two sp^2 orbitals along the bond axis generate the σ-bond; the overlap of two p orbitals gives the π-bond.

In conjugated systems, the π-bonds are close enough to each other, their wave functions overlap and π-electrons are allowed to move along the conjugation path. The elec-

tronic structure of the overlapping π-orbitals resembles the band structure of inorganic semiconductors, in which two energy levels, the conduction and the valence band, are separated by a region of forbidden energies. In conjugated systems, the two bands are replaced by the delocalized bonding and antibonding π-orbitals, the former filled with electrons (up to the highest occupied molecular orbital, HOMO), the latter empty (starting from the lowest unoccupied molecular orbitals, LUMO), with an energy band-gap separating the two. However, the concept of band conduction does not apply to organic semiconductors: the delocalization of electronic states in organic semiconductors is only within the molecules, and do not extend to the whole material. Due to the disordered configuration of conjugated polymers and molecules, organic semiconductors are typically subject to energetic disorder, and the HOMO and LUMO levels are a distribution of localized states.

1.4 Organic photovoltaic devices

A typical OPV device consists of a photoactive layer sandwiched between two electrodes, one of which has to be transparent to allow the incoming light to reach the photoactive layer. The absorption of light excites electrons into the LUMO of the absorber material, creating strongly bound electron-hole pairs called excitons. The excitons have to overcome their binding energy to dissociate; in the absence of a mechanism to dissociate the excitons, they will spontaneously decay. Efficient photocurrent generation in an organic device was first reported by Tang in 1986,[19] employing a vacuum-deposited copper phthalocyanine (CuPc)/perylene derivative donor/acceptor bilayer device. The difference in electronic affinities between these two materials creates an energy offset at their interface, driving exciton dissociation.

Similar to this early device, many OPVs have an active layer which consist of two materials, one electron donor and one electron acceptor (Figure 1.3). In most of the state-of-the-art organic solar cells, the donor material is a conjugated polymer and the acceptor material is a fullerene derivative.[20,21] Once the excitons are generated in the absorber material, they need to reach the donor:acceptor interface to be dissociated. The lifetime of excitons is finite, and so is their diffusion length, which is around 10 nm in conjugated molecules.[22,23] If the donor:acceptor interface is too far from the point where an exciton is generated, this exciton will decay before reaching the interface and will not yield free charge carriers. The diffusion of excitons is a severe limit for the performance of donor:acceptor bilayer. On one hand, the thickness of the photoactive layer has to be around 100 nm to efficiently absorb light; on the other hand, in a bilayer 100 nm thick, only a small fraction of the excitons would be generated close enough to the donor:acceptor interface. One solution to this problem has been provided in 1995 with the so-called bulk heterojunction (BHJ) solar cell.[24,25] The BHJ concept involves the self-assembly of nanoscale heterojunctions by spontaneous phase separation of the donor and the acceptor material. As a result of this self-assembly, charge-separating heterojunctions are formed throughout the bulk of the material.[24]

Excitons that diffuse to the donor:acceptor interface can dissociate into free electrons and holes. Connecting the device to an external circuit, the free charge carriers are then transported to the contacts and extracted from the device, thus generating an electric current. Negative and positive charges are present in the photoactive layer at the same time; thus, there is a certain probability of having recombination of charges. Recombination represents a loss process for a photovoltaic device, because it reduces the number of charge carriers that contribute to the photocurrent.

There are three fundamental processes that govern the operation of an OPV device: the generation, the transport, and the recombination of charge carriers. The understanding of the basic physical phenomena is crucial for the optimization of the performance and the stability of the devices.

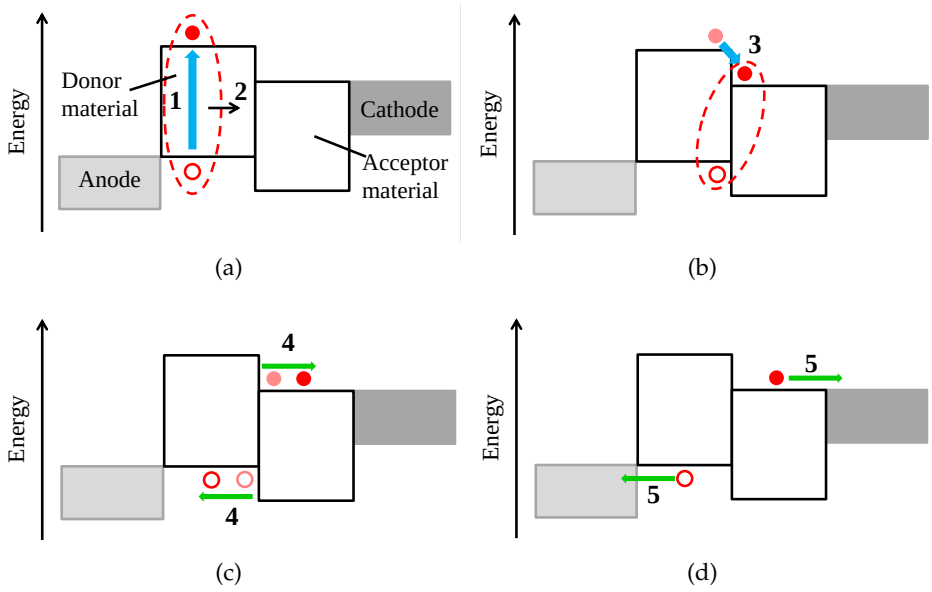

Figure 1.3: Schematic working of an OPV device. a) absorption of light generates an exciton (1), which eventually diffuses towards the donor:acceptor interface (2); b) the exciton is dissociated *via* charge-transfer (3) and a bound electron-hole pair (charge transfer state, CT) may be formed; c) a further dissociation step (4) yields free charge carriers; d) the carriers are transported to the electrodes (5). The full circles represent an electron, the empty circles represent a hole. The anode is the contact whose work function aligns with the HOMO level of the donor material.

1.4.1 Generation of free charges

The overall generation rate of free charges, G, depends on the efficiency of the optical absorption and on the efficiency of the dissociation of the photogenerated excitons into free charges. The absorption can be modelled by taking into account the interference between the incoming light and the radiation reflected by the opaque electrode;[26] several optical models involve the transfer matrix formalism.[27]

The dissociation of excitons has a fundamental importance on the charge generation process. Nevertheless, the exact mechanism through which excitons dissociate into free charges are not fully understood yet, and the subject is still highly debated.[28–30] The formation of charge transfer states (CT) has been reported in several bulk heterojunctions.[31] CT states are the result of the dissociation of excitons at the donor:acceptor interface. The electron and hole forming a CT state are localized on the acceptor and donor material, respectively, but they are still bound by Coulombic force;[32] further dissociation of the CT states is needed to obtain free electrons and holes.

An electron-hole pair is defined to be dissociated once the distance between the charges exceeds the capture radius, which is the distance at which the mutual Coulomb attraction between the charges becomes negligible compared to the energetic disorder. If the electron and hole generated from the same exciton do not overcome their coulombic attraction, they recombine. This recombination process is referred to as geminate recombination and it has been observed for both small molecule and polymer semiconductors.[33,34] Also CT recombination has been demonstrated to be detrimental for the overall efficiency of the device.[35,36]

1.4.2 Charge transport

Energetic and spatial disorder in organic semiconductors causes charge transport to occur via hopping between localized states (Figure 1.4).[37,38] This charge transport mechanism is characterized by lower electron and hole mobilities compared to the values that are found for inorganic semiconductors. The mobility of the charge carriers is a measure of their ability to move through the material in response to an electric field. When the transport of charge is an hopping process, the mobility depends on the hopping rates.

Hopping rate expressions describe the rate at which a particle at site i will hop to another site j, and depend on the spatial distance and the total site energy difference between the initial and final sites. The most commonly used rate expression was derived by Miller and Abrahams:[39]

$$\nu_{ij} = \nu_0 \exp\left(-2\alpha r_{ij} - \frac{\Delta E_{ij} + |\Delta E_{ij}|}{2k_B T}\right), \tag{1.3}$$

here ΔE_{ij} contains the energy difference between to sites, k_B is the Boltzmann constant, T is the temperature, ν_0 is the attempt to jump frequency, r_{ij} is the intersite distance and α is the inverse delocalization length. The semi classical expression is based on single phonon-assisted hopping, and was derived for describing charge hopping through

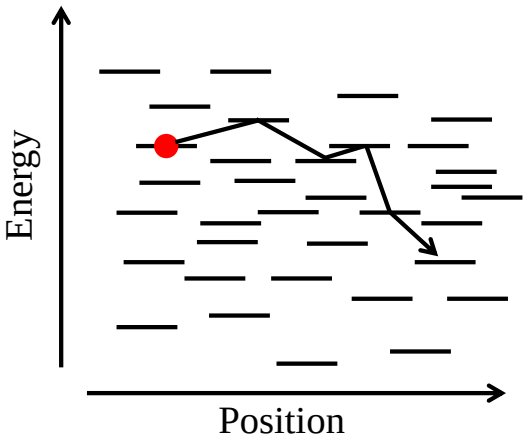

Figure 1.4: Hopping through a disordered density of states. The energy distribution of the density of states (DOS) is generally assumed to be a gaussian.

shallow trap states in crystalline semiconductors at low temperatures. Charge carrier transport calculations that are based on this relations explain the dependence of temperature,[40] charge carrier mobility on electric field and carrier density.[41] Another important semi-classical approach was developed by Marcus:[42]

$$\nu_{ij} = \nu_0 \sqrt{\frac{\pi}{4\lambda k_B T}} \exp\left(-2\alpha r_{ij} - \frac{\left(\Delta E_{ij} + \lambda\right)^2}{4\lambda k_B T} \right). \tag{1.4}$$

This expression assumes that the initial and final sites are located in a potential well, separated by an energy barrier. The size of the energy barrier is provided by the reorganization energy λ. The introduction of such barrier mimics the polaronic nature of charge carriers in the organic semiconductors: charges distort their close surroundings and are therefore located in a potential well. Charges hop from well to well, and have to overcome the barrier in between.

Semi-classical approaches break down when $T \rightarrow 0$ K: both Miller-Abrahams and Marcus hopping predict that the charge carrier mobility decreases as a function of electric field and that the charge carrier mobility vanishes for temperatures close to 0K.[43] Alternatively, quantum mechanical descriptions are able to deal with these situations. An example of a quantum mechanical hopping rate expression is nuclear tunnelling mediated hopping.[44] This hopping model assumes that the system always possesses a ground state energy that drives the hopping process, even at 0K. This results in a non-vanishing mobility for temperatures down to 0K. For increased temperatures, the quantum mechanical expression reduces to the semi-classical Marcus expressions.

The first theoretical description of the charge carrier mobility in disordered organic semiconductors was given by Bässler in 1993, by considering the charge transport process as a Miller-Abrahams hopping in a gaussian DOS.[45] By means of Monte Carlo simulations, Bässler proposed the following expression for the charge mobility:

$$\mu = \mu_\infty \exp\left[-\left(\frac{2\sigma}{3k_BT}\right)^2\right] \times \begin{cases} \exp\left(C[(\sigma/k_BT)^2 - \Sigma^2]\sqrt{F}\right); & \Sigma \geq 1.5 \\ \exp\left(C[(\sigma/k_BT)^2 - 2.25^2]\sqrt{F}\right); & \Sigma < 1.5 \end{cases} \tag{1.5}$$

Here, μ_∞ is the mobility in the limit $T \to \infty$, σ is the variance of the gaussian DOS, C is a constant dependent on the site spacing (typically $1 - 2$ nm in organic semiconductors), Σ is the degree of positional disorder, and F is the electric field.

The mobility described by Bässler is dependent on the temperature and on the electric field. Later, it was discovered that the charge carrier density also influences the mobility.[46] In 2005, Pasveer *et al.* provided a full description of the mobility in organic diodes, including the effects of both charge density and electric field.[41]

For some donor:acceptor blends, the transport of either electrons or holes can be limited by charge trapping. A charge trap is a defect site within the forbidden energy gap of the donor:acceptor blend.[47] Charge trapping is often a limitation for the transport of electrons in conjugated polymers.[48] Analysing the trap-limited electron transport in different conjugated polymer, Nicolai *et al.* found that all exhibit a common trap distribution, located at an energy of 3.6 eV below the vacuum level,[49] indicating that the trap states have a common origin. Although the origin of the electron-trapping states is not known, it is likely that they are due to chemical defects related to water or oxygen.[50,51] Trapping of holes has been shown to be less significative, although recent studies provided experimental evidences for hole trapping in organic materials.[52,53]

1.4.3 Charge recombination

An important loss mechanism in organic solar cells is the non-geminate recombination of free charges. The process of bimolecular recombination has been first described by Langevin for ions in a gas;[54] the rate of the bimolecular recombination depends quadratically on the charge density and it is determined by the time required for electrons and holes to diffuse towards each other.[55] The rate of bimolecular recombination is given by

$$R_{\text{bimolecular}} = \gamma(np - n_i^2), \tag{1.6}$$

where n and p are the density of electrons and holes respectively, n_i is the intrinsic carrier concentration of electron and holes and γ is the bimolecular recombination coefficient. According to Langevin's theory, the bimolecular recombination coefficient is given by,[54]

$$\gamma_L = \frac{q}{\varepsilon}(\mu_n + \mu_p). \tag{1.7}$$

Here, q is the elementary charge, ε is the dielectric constant of the donor:acceptor blend, and $\mu_{n(p)}$ the electron (hole) mobility. The subscript L in the recombination coefficient denotes that this is the bimolecular recombination coefficient that follows from Langevin's theory. However, in many organic solar cells a bimolecular recombination rate significantly lower than the one predicted by Langevin's expression has been reported.[56–58] Langevin's equation can still be used to describe bimolecular recombination in organic BHJs, but it is necessary to apply a prefactor $\gamma_{\mathrm{pre}} \leq 1$:

$$\gamma = \gamma_{\mathrm{pre}}\gamma_L = \gamma_{\mathrm{pre}}\frac{q}{\varepsilon}\left(\mu_n + \mu_p\right), \tag{1.8}$$

with γ the total recombination strength.

If charge traps are present, an additional recombination channel is active, the description of which is given by the Shockley-Read-Hall (SRH) equation:[59,60]

$$R_{\mathrm{SRH}} = \frac{C_n C_p N_t}{[C_n(n + n_i) + C_p(p + p_i)]}, \tag{1.9}$$

where R_{SRH} is the rate of trap-assisted recombination, $C_{n(p)}$ is the capture coefficient for electrons (holes), respectively, and N_t is the density of charge traps.

Furthermore, recombination losses due to surface recombination may have a significant impact on the device performance.[61–64] Surface recombination is governed by the presence of minority carriers at a contact. Electrons (holes) diffusing to the anode (cathode) recombine with injected holes (electrons). Thus, the current at the electrodes is related to the density of minority carriers:[62,65]

$$J_{n(p)} = qS_{n(p)}[n(p) - n(p)_{eq}], \tag{1.10}$$

where $J_{n(p)}$ is the electron (hole) current at the anode (cathode), $S_{n(p)}$ is the surface recombination velocity, and $n(p)_{eq}$ is the equilibrium carrier density at the contact. In many models, the surface recombination velocity is (implicitly) assumed to be infinite, meaning that the densities of carriers at the contacts are equal to their equilibrium values.[66,67]

1.5 The influence of the morphology

The morphology of the interpenetrating network of donor and acceptor material in BHJs is relevant to the processes of generation, transport and recombination of free charges.[68–70] The length scale of the phase separation has to be smaller than the exciton diffusion length, so that all the excitons have the possibility to reach the donor:acceptor interface before decaying. Beside the capability of generating free charge carriers, no less

important is the existence of pathways to extract these carriers from the device.[71,72] The ideal network of donor and acceptor has to be bicontinuous, providing percolation pathways for both electrons and holes, generated in any point of the layer, to reach the electrodes. Too fine a phase separation would hinder the transport of charges, slowing them down on their way towards the electrodes and increasing the probability that charges of opposite sign would meet each other and recombine. Also the composition[70,73,74] and the crystallinity[75,76] of the donor and acceptor domains play an important role in determining how easily the charge will be generated and transported.

Control over the morphology of the active layer can be achieved by varying the processing conditions of the materials.[77] Organic photovoltaic devices are typically produced by solution-based processes, such as spin-casting, or vacuum-based deposition. A vast number of publications qualitatively addresses the importance of the choice of solvent,[78–80] co-solvent[77,81] and additives,[82] as well as the effect of post-fabrication treatments, *e.g.* thermal[83] and solvent[84] annealing. Depending on the processing conditions, the active layer can exhibit a morphology which varies between an extremely finely dispersed mixture of donor and acceptor to a coarse phase-separated film.

1.6 Fabrication and characterization of the devices

In this section the fabrication and characterization techniques used in this thesis are presented. First, we show the structure of the typical devices produced in our laboratory. Then, we describe the steady-state characterization techniques employed for organic solar cells and single carrier devices.

1.6.1 Solar cells

The typical structure of a BHJ solar cell is shown in Figure 1.5a.

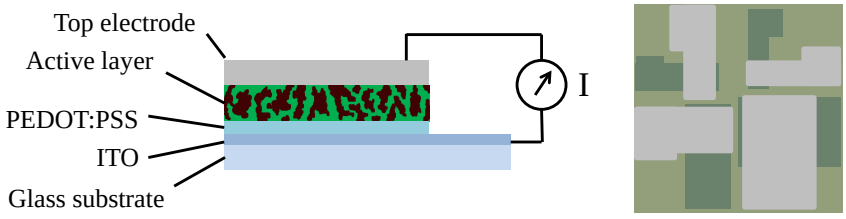

Figure 1.5: a) Typical structure of a conventional BHJ solar cell; b) the top view of the samples produced in our lab.

The devices shown in this thesis are realized on 3 x 3 cm glass substrates with a prepatterned indium tin oxide (ITO) layer. The substrates are thoroughly cleaned by washing with detergent solution and ultrasonication in acetone and isopropyl alcohol, followed by UV-ozone treatment. To reduce the roughness of the anode and improve the work function, a thin layer of poly(3,4-ethylene dioxythiophene):poly(styrene sulfonate) (PEDOT:PSS) is spin cast on the substrate. After removing all the water from the PEDOT:PSS layer through a short baking step, the substrates are transferred to inert atmosphere, where the active layer is spin cast. Unless stated differently, the deposition of the active layer occurs from a solution which contains both the donor and the acceptor. If an annealing step is necessary, it is performed after the spin casting of the blend and before the deposition of the top contact. The devices are finished by thermal evaporation of the cathode, usually consisting of 1 nm of LiF and 100 nm of Al. The shadow mask used for the evaporation of the cathode creates a pattern that overlap with the ITO bottom contact, defining the active layer of the solar cells (Figure 1.5(b)). Each substrate contains four device, with active areas in the range $10^{-5} - 10^{-4}$ m^2.

1.6.2 Single carrier devices

To characterize the transport of holes and electrons, single carrier devices are fabricated by sandwiching the active layer between selective contacts that suppress the injection of either electrons or holes. To do so, contact materials with appropriate work function, either close to the LUMO or to the HOMO of the organic layer, have to be employed. The fabrication process is similar to the one described for solar cells. For single carrier devices, the bottom contact is thermally evaporated on glass substrates. To reduce the series resistance, the shadow masks used for single carrier devices define four small active areas (10^{-6} m^2). The typical structure for hole-only devices is Cr(1 nm)/Au(20 nm)/PEDOT:PSS/active layer/Pd(15 nm)/Au(80 nm). For electron-only devices, the typical structure is Al(20 nm)/active layer/LiF(1 nm)/Al(100 nm).

1.6.3 Current-voltage characteristics

In order to measure the electrical characteristics of the devices, current-voltage measurements are performed in nitrogen atmosphere using a computer controlled Keithley 2400 SourceMeter. The current density flowing through the device (J) is measured as a function of the applied bias V. Here, a positive V corresponds to positive biasing of the anode. The obtained curve is the JV characteristic of the device. For single carrier devices, the JV curves are recorded in dark, and the mobilities of the charge carriers are determined using the space-charge limited current (SCLC) method, which is described in Section 2.3.1.

For solar cells, the JV curves are measured both in dark and under illumination, using a Steuernaugel SolarConstant 1200 metal halide lamp. The spectrum of the illumination source used for the measurement of the JV curve in light is not the same as the AM1.5 spectrum; to accurately measure the efficiency of the device at 1 sun, the spectral

response of the sample is measured using pulsed monochromatic illumination by means of a chopped light beam and a SR830 lock-in amplifier. The spectrum of the lamp, the AM1.5 spectrum and the spectral responses of the sample and of a reference Si diode are used to calculate the mismatch factor.[85] Then, the solar simulator is set to 1 sun using the reference Si diode. Details of the calibration procedure can be found in Ref. 85.

1.7 Modelling of BHJ devices

The performance of organic solar cells has increased rapidly in the past two decades.[10,78,86,87] Developments are driven by design and engineering of new materials, but also by improving fabrication conditions and device structure. Stretching the limits even further requires physical insight in the mechanisms involved in the device operation. The joint effect of all processes makes it difficult to directly distinguish between separate effects. Numerical simulations allow to overcome these issues, because the influence of different mechanisms can be studied independently. The ultimate goal of simulations is to become predictive: predicting the performance of certain materials or configurations, without even having to produce these first.

Simulations of charge transport in organic semiconductors originate from 1D drift-diffusion calculations that were first introduced in the 1964 for describing charge transport in inorganic semiconductors.[88] Solving systems of coupled non-linear equations has become a fast and well understood method to obtain insight in the macroscopic device physics of semiconductor devices. The ease at which this type of simulation can be implemented also made it attractive for modelling the transport in organic light emitting diodes[89] and solar cells.[90] Many features that are specific to organic semiconductors were added: mobility models that provide an improved description of the charge transport,[41] exciton transport[91] and charge separation mechanisms.[90] For organic bulk heterojunctions, 1D drift-diffusion simulations use an effective medium approach: the effective medium is made up by the electron transporting level of the acceptor and the hole transporting level of the donor. This allows for fast calculations, but neglects the influence of morphology. On the contrary, 2D and 3D simulations contain a separate donor and acceptor phase, enabling calculations to determine the influence of morphology.[92] Although drift-diffusion simulations are capable to provide a good macroscopic description of the device operation, some phenomena require a more fundamental approach. For instance, a description in terms of charge carrier densities is unable to properly include particle-particle interactions between separate charges, and to treat exciton separation on a microscopic scale. As a solution, kinetic Monte Carlo simulations allow 3D treatment on molecular level.[45,93]

1.7.1 Details of drift-diffusion simulations

The band diagram of a donor:acceptor bulk heterojunction solar cell at short-circuit conditions is shown in Figure 1.6. The excitons are dissociated into free charges thanks to the

energy offset between the LUMOs or between the HOMOs of the two materials. Once free electrons and holes are present in the device, they move driven by the built-in and the external electric field (drift) and by their concentration gradient (diffusion).

A widely used approach to the simulation of organic semiconductor devices consist in considering the effects of both drift and diffusion on the transport of charges (drift-diffusion simulations).

The electric field is obtained by solving the Poisson equation:[94]

$$\frac{\partial^2 \psi(x)}{\partial x^2} = \frac{q}{\varepsilon} \left[n(x) - p(x) \right], \tag{1.11}$$

where ψ is the electric potential. In our notation, x denotes the distance from the cathode.

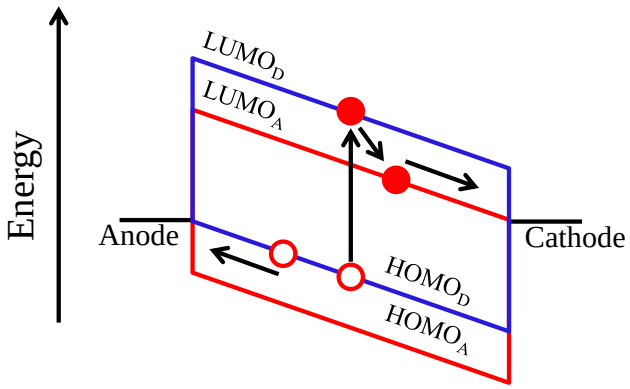

Figure 1.6: Band diagram of a bulk heterojunction solar cell at short-circuit conditions (for simplicity, any band bending is ignored). The notation D and A refers to donor and acceptor material, respectively.

From the conservation of charges, the continuity equations for the electrons and holes in the steady state are derived:[94]

$$\frac{\partial J_n(x)}{\partial x} = q\,(G - R) \tag{1.12a}$$

$$\frac{\partial J_p(x)}{\partial x} = -q\,(G - R)\,. \tag{1.12b}$$

Here, $J_{n(p)}$ is the electron (hole) current density, G and R are the rate of generation and recombination of free charges, respectively. By incorporating the drift and diffusion terms, the expressions for the electron and hole current densities read[94]

$$J_n = -qn\mu_n \frac{\partial \psi(x)}{\partial x} + qD_n \frac{\partial n(x)}{\partial x} \tag{1.13a}$$

$$J_p = -qp\mu_p \frac{\partial \psi(x)}{\partial x} - qD_p \frac{\partial p(x)}{\partial x}, \tag{1.13b}$$

where $D_{n(p)}$ are the carrier diffusion coefficients, which are related to the mobilities of the two species through the classical or the generalized Einstein relation.[95–97]

Although the absorption of light, and hence the generation rate G, is generally not uniform across the active layer, it has been shown that including an optical profile in the modelling of the device does not, in general, significantly change the results for thickness of the active layer lower than 300 nm.[98] Thus, a constant generation profile through the active layer can be used if the profile is not available.

The system of Equations $1.11 - 1.13$ has to be solved to calculate the total current extracted from the device. To do so, it is necessary to introduce boundary conditions that specify the carrier densities and the potential at both contacts. The boundary condition on the potential is given by

$$q\left(V(L) - V(0) + V\right) = W_{\text{anode}} - W_{\text{cathode}}, \tag{1.14}$$

where $V(L)$ and $V(0)$ are the potentials at the two electrodes, W_{anode} and W_{cathode} are the work functions of the anode ($x = L$) and the cathode ($x = 0$), respectively. The boundary conditions on the electron and hole densities at the contacts depends on the type of contacts and on the surface recombination velocity. For ohmic contacts (no energy barrier for the injection of charges) and infinite surface recombination velocity, the boundary conditions are given by

$$n(0) = p(L) = N_{cv} \tag{1.15a}$$

$$n(L) = N_{cv} \exp\left(-\frac{E_{\text{gap}}}{k_B T}\right) \tag{1.15b}$$

$$p(0) = N_{cv} \exp\left(-\frac{E_{\text{gap}}}{k_B T}\right), \tag{1.15c}$$

where N_{cv} is the effective density of states and E_{gap} is the effective bandgap ($E_{\text{gap}} = \text{LUMO}_A - \text{HOMO}_D$).

The equations above are written in one dimension (1D); by solving them, it is implied that the charges move only in the direction x, normal to the surface of the device. Moreover, the 1D approach treats the active layer as an effective blend, in which every node can be at the same time donor and acceptor, thus neglecting the effect of the morphology on the device performance.

In order to include the effects of the blend microstructure in drift-diffusion simulations, one has to leave the 1D approach and add one or two more dimensions. The morphology of the blend is simulated by means of a 2D or 3D grid, in which each node represents either the donor or the acceptor phase, or, eventually, a mixed phase of the two materials.

Furthermore, the number of excitons that yield free charges at the interface is calculated by solving the exciton diffusion equation

$$0 = -\frac{X(\vec{r})}{\tau} + D_x \nabla^2 X(\vec{r}) + g, \tag{1.16}$$

where $X(\vec{r})$ is the exciton density in the position defined by the vector $(\vec{r})$, τ is the exciton lifetime, D_x is the exciton diffusion constant and g is the generation rate of excitons. We note that the exciton diffusion equation can be also solved for the 1D case, if a bilayer device is considered.[99]

The numerical solution of the 2D or 3D equations involves the discretization of the equations over 2D or 3D grids and requires a significantly larger computational effort. At the price of longer simulation times than in the 1D case, the implementation of 2D and 3D models can provide insight in the effect of the morphology on the device performance.

1.8 Outline of this thesis

In the last years the efficiency of organic photovoltaics greatly improved, exceeding 10%. At the same time, more stable materials and device architectures have been designed. The commercialization of OPVs requires the simultaneous achievement of both the desired characteristics, efficiency and stability. This thesis deals with the physics of organic solar cells, aiming at providing insight into the mechanisms that limits the performance and the stability of the devices.

The first part of this thesis regards the morphology - efficiency relation. In **chapter 2** the electrical properties of the donor:acceptor system PDPP5T:[70]PCBM are experimentally characterized. Depending on the processing conditions, this system can yield many different morphologies, which are representative of a large number of BHJ devices. It is thus an ideal system to study how the morphology influences the generation, transport and recombination of charges. The experimental results are used in **chapter 3** to model the JV characteristics of PDPP5T:[70]PCBM devices with either homogeneous or coarsely phase-separated morphology. For the latter case, a simple model is presented, which describe the current extracted from the device as the sum of two contributions, flowing in parallel through the active layer.

The "parallel model" presented in chapter 3 is validated in **chapter 4** by comparing its results with those given by three dimensional (3D) drift-diffusion model. Both the models are used to simulate the effect of large compositional heterogeneities on the performance of BHJ solar cells.

Chapter 5 introduces a figure of merit for the fill factor of bulk heterojunction solar cells. Unlike J_{sc} and V_{oc}, a clear understanding of what determines FF is still lacking, making targeted improvement difficult. After quantifying the recombination and extraction rates of charge carriers, it is shown how the FF is dependent on the ratio of these two quantities. The results of drift-diffusion simulations are compared with a large number of experimental data, which include many different donor:acceptor combinations.

Finally, **chapter 6** is dedicated to the stability of OPVs. In particular, the degradation induced by UV light is treated in this chapter. Experimental work carried out on one of the most promising blend in term of efficiency, PTB7:[70]PCBM, indicates that the efficiency of this system rapidly decreases when the devices are exposed to UV light, even in the absence of oxygen and water. Although the fullerene derivative [70]PCBM is used as acceptor in many state-of-the art OPVs, it is shown here that it may give rise to stability issues, *e.g.* when blended with PTB7, and therefore one of the goals in the design of new donor materials has to be the compatibility with [70]PCBM under UV light.

References

[1] S. Shafiee, E. Topal, *Energy policy* **2009**, *37*, 181.

[2] O. Ellabban, H. Abu-Rub, F. Blaabjerg, *Renewable Sustainable Energy Rev.* **2014**, *39*, 748.

[3] www.iea.org/publications/freepublications/publication/KeyWorld2014.pdf accessed on 01/10/2015.

[4] www.nrel.gov/ncpv/images/`efficiency_chart`.jpg accessed on 01/10/2015.

[5] R. Søndergaard, M. Hösel, D. Angmo, T. T. Larsen-Olsen, F. C. Krebs, *Mater. Today* **2012**, *15*, 36.

[6] M. Kaltenbrunner, M. S. White, E. D. Głowacki, T. Sekitani, T. Someya, N. S. Sariciftci, S. Bauer, *Nature Commun.* **2012**, *3*, 770.

[7] K. S. Chen, H. L. Yip, J. F. Salinas, Y.-X. Xu, C.-C. Chueh, A. K.-Y. Jen, *Adv. Mater.* **2014**, *26*, 3349.

[8] A. L. Roes, E. A. Alsema, K. Blok, M. K. Patel, *Prog. Photovolt: Res. Appl.* **2009**, *17*, 372.

[9] O. Synooka, K.-R. Eberhardt, H. Hoppe, *RSC Adv.* **2014**, *4*, 16681.

[10] Y. Liu, J. Zhao, Z. Li, C. Mu, W. Ma, H. Hu, K. Jiang, H. Lin, H. Ade, H. Yan *Nature Commun.* **2014**, *5*, 5293.

[11] J. You, L. Dou, K. Yoshimura, T. Kato, K. Ohya, T. Moriarty, K. Emery, C.-C. Chen, J. Gao, G. Li, Y. Yang, *Nature Commun.* **2013**, *4*, 1446.

[12] H. Mette, H. Pick *Z. Physik* **1953**, *134*, 566.

[13] H. Kallmann, M. Pope, *J. Chem. Phys.* **1959**, *30*, 585.

[14] C. K. Chiang, C. R. Fincher Jr, Y. W. Park, A. J. Heeger, H. Shirakawa, E. J. Louis, S. C. Gau, A. G. MacDiarmid, *Phys. Rev. Lett.* **1977**, *39*, 1098.

[15] J. H. Burroughes, D. D. C. Bradley, A. R. Brown, R. N. Marks, K. Mackay, R. H. Friend, P. L. Burns, A. B. Holmes, *Nature* **1990**, *347*, 539.

[16] N. S. Sariciftci, D. Braun, C. Zhang, V. I. Srdanov, A. J. Heeger, G. Stucky, F. Wudl, *Appl. Phys. Lett.* **1993**, *62*, 585.

[17] G. A. Chamberlain, *Solar cells* **1983**, *8*, 47.

[18] W. Brütting,S. Berleb, A. G. Mückl, *Organic Electron.* **2001**, *2*, 1.

[19] C. W. Tang, *Appl. Phys. Lett.* **1986**, *48*, 183.

[20] C. J. Brabec, S. Gowrisanker, J. J. M. Halls, D. Laird, S. Jia, S. P. Williams, *Adv. Mater.* **2010**, *22*, 3839.

[21] T. Liu, A. Troisi, *Adv. Mater.* **2013**, *25*, 1038.

[22] O. V. Mikhnenko, H. Azimi, M. Scharber, M. Morana, P. W. M. Blom, M. A. Loi, *Energy Environ. Sci.* **2012**, *5*(5), 6960.

[23] S. D. Dimitrov, C. B. Nielsen, S. Shoaee, P. Shakya Tuladhar, J. Du, I. McCulloch, J. R. Durrant, *J. Phys. Chem. Lett.* **2011**, *3*, 140.

[24] G. Yu, J. Gao, J. C. Hummelen, F. Wudl, A. J. Heeger, *Science* **1995**, *270*, 1789.

[25] J. Halls, C. Walsh, N. Greenham, E. Marseglia, R. Friend, S. Moratti, A. Holmes, *Nature* **1995**, *270*, 498.

[26] G. F. Burkhard, E. T. Hoke, M. D. McGehee *Adv. Mater.* **2010**, *22*, 3293.

[27] L. A. A. Pettersson, L. S. Roman, O. Inganäs, *J. Appl. Phys.* **1999**, *86*, 487.

[28] G. Grancini, M. Maiuri, D. Fazzi, A. Petrozza, H.-J. Egelhaaf, D. Brida, G. Cerullo, G. Lanzani, *Nat. Mater.* **2013**, *12*, 29.

[29] B. Kraabel, D. McBranch, N. S. Sariciftci, D. Moses, A. J. Heeger, *Phys. Rev. B* **1194**, *50*, 18543.

[30] S. Few, J. M. Frost, J. Nelson, *Phys. Chem. Chem. Phys.* **2015**, *17*, 2311.

[31] C. Piliego, M. A. Loi, *J. Mater. Chem.* **2012**, *22*, 4141.

[32] M. Pope, C. E. Swenberg, *Electronic Process in Organic Crystals*. 2nd ed. Oxford University Press, Claredon Press, Oxford, 1982.

[33] B. Schweitzer, V. I. Arkhipov, U. Scherf, H. Bässler, *Chem. Phys. Lett.* **1999**, *313*, 57.

[34] D. Credgington, F. C. Jamieson, B. Walker, T.-Q. Nguyen, J. R. Durrant, *Adv. Mater.* **2012**, *24*, 2135.

[35] M. C. Scharber, C. Lungenshmied, H.-J. Egelhaaf, G. Matt, M. Bednorz, T. Fromherz, J. Gao, D. Jarzab, M. A. Loi, *Energy Environ. Sci.* **2011**, *4*, 5077.

[36] M. C. Scharber, M. Koppe, J. Gao, F. Cordella, M. A. Loi, P. Denk, M. Morana, H.-J. Egelhaaf, K. Forberich, G. Dennler, R. Gaudiana, D. Waller, Z. Zhu, X. Shi, C. J. Brabec, *Adv. Mater.* **2010**, *22*, 367.

[37] N. F. Mott, *Can. J. Phys.* **1956**, *34*, 1356.

[38] E. M. Conwell, *Phys. Rev.* **1956**, *103*, 51.

[39] A. Miller, E. Abrahams, *Phys. Rev.* **1960**, *120*, 745.

[40] S. D. Baranovskii, I. P. Zvyagin, H. Cordes, S. Yamasaki, P. Thomas, *Phys. Stat. Sol.(b)* **2002**, *230*, 281.

[41] W. F. Pasveer, J. Cottaar, C. Tanase, R. Coehoorn, P. A. Bobbert, P. W. M. Blom, D. M. De Leeuw, M. A. J. Michels, *Phys. Rev. Lett.* **2005**, *94*, 206601.

[42] R. A. Marcus, N. Sutin, *Biochim. Biophys. Acta* **1985**, *811*, 265.

[43] J. D. Yuen, R. Menon, N. E. Coates, E. B. Namdas, S. Cho, S. T. Hannahs, D. Moses, A. J. Heeger, *Nature Mater.* **2009**, *8*, 572.

[44] K. Asadi, A. J. Kronemeijer, T. Cramer, L. J. A. Koster, P. W. M. Blom, D. M. de Leeuw, *Nature Commun.* **2013**, *4*, 1710.

[45] H. Bässler, *Phys. Status Solidi b* **1993**, *175*, 15.

[46] M. C. J. M. Vissenberg, M. Matters, *Phys. Rev. B* **1998**, *57*, 12964.

[47] M. A. Lampert, *Phys. Rev.* **1956**, *103*, 1648.

[48] M. M. Mandoc, B. de Boer, G. Paasch, P. W. M. Blom, *Phys. Rev. B* **2007**, *75*, 193202.

[49] H. T. Nicolai, M. Kuik, G. A. H. Wetzelaer, B. De Boer, C. Campbell, C. Risko, J. L. Brédas, P. W. M. Blom, *Nature Mater.* **2012**, *11*, 882.

[50] H.-E. Tseng, K.-Y. Peng, S.-A. Chen, *Appl. Phys. Lett.* **2003**, *82*, 4086.

[51] V. Kažukauskas, *Semicond. Sci. Technol.* **2004**, *19*, 1373.

[52] J. Schafferhans, A. Baumann, C. Deibel, V. Dyakonov, *Appl. Phys. Lett.* **2008**, *93*, 093303.

[53] H. S. Woo, R. Czerw, S. Webster, D. L. Carroll, J. Ballato, A. E. Strevens, D. O'Brien, W. J. Blau, *Appl. Phys. Lett.* **2000**, *77*, 1393.

[54] P. Langevin, *Ann. Chim. Phys* **1903**, *28*, 122.

[55] G. J. Adriaenssens, V. I. Arkhipov, *Sol. State Commun.* **1997**, *103*, 541.

[56] G. Juška, K. Arlauskas, J. Stuchlik, R. Österbacka, *J. Non-Cryst. Solids* **2006**, *352*, 1167.

[57] A. Facchetti, *Mater. Today* **2013**, *16*, 123.

[58] P. Zalar, M. Kuik, N. A. Ran, J. A. Love, T.-Q. Nguyen, *Adv. Energy Mater.* **2014**, *4*, 1400438.

[59] W. Shockley, W. T. Read Jr, *Phys. Rev.* **1952**, *87*, 835.

[60] R. N. Hall, *Phys. Rev.* **1952**, *87*, 387.

[61] A. Wagenpfahl, C. Deibel, V. Dyakonov, *J. Sel. Topics Quantum Electron.* **2010**, *16*, 1759.

[62] T. Kirchartz, B. E. Pieters, K. Taretto, U. Rau, *Phys. Rev. B* **2009**, *80*, 035334.

[63] J. Nelson, *Phys. Rev. B* **2003**, *67*, 155209.

[64] J. C. Scott, G. G. Malliaras, *Chem. Phys. Lett.* **1999**, *299*, 115.

[65] J. Kniepert, I. Lange, N. J. van der Kaap, L. J. A. Koster, Neher D. *Adv. Energy Mater.* **2014**, *4*, 1301401.

[66] C. Deibel, A. Wagenpfahl, V. Dyakonov, *Phys. Status Solidi RRL* **2008**, *2*, 175.

[67] S. Lacic, O. Inganäs, *J. Appl. Phys.* **2005**, *97*, 124901.

[68] M. Dante, A. Garcia, T.-Q. Nguyen, *J. Phys. Chem. C* **2009**, *113*, 1596.

[69] J. Guo, H. Ohkita, H. Benten, S. Ito, *J. Am. Chem. Soc.* **2010**, *132*, 6154.

[70] B. A. Collins, Z. Li, J. R. Tumbleston, E. Gann, C. R. McNeill, H. Ade, *Adv. Energy Mater.* **2013**, *3*, 65.

[71] J. A. Bartelt , Z. M. Beiley, E. T. Hoke, W. R. Mateker, J. D. Douglas, B. A. Collins, J. R. Tumbleston, K. R. Graham, A. Amassian, H. Ade, J. M. J. Fréchet, M. F. Toney, M. D. McGehee, *Adv. Energy Mater.* **2013**, *3*, 364.

[72] L. J. A. Koster, *Phys. Rev. B* **2010**, *81*, 205318.

[73] C. R. McNeill, B. Watts, L. Thomsen, W. J. Belcher, N. C. Greenham, P. C. Dastoor, *Nano Lett.* **2006**, *6*, 1202.

[74] B. A. Collins, E. Gann, L. Guignard, X. He, C. R. McNeill, H. Ade, *J. Phys. Chem. Lett.* **2010**, *1*, 3160.

[75] W. C. Tsoi, S. J. Spencer, L. Yang, A. M. Ballantyne, P. G. Nicholson, A. Turnbull, A. G. Shard, C. E. Murphy, D. D. C. Bradley, J. Nelson, J.-S. Kim, *Macromol.* **2011**, *44*, 2944.

[76] M. J. Im, S. Y. Son, B. J. Moon, G.-Y. Lee, J. H. Kim, T. Park, *Organic Electron.* **2013**, *14*, 3046.

[77] M. M. Wienk, M. Turbiez, J. Gilot, R. A. J. Janssen, *Adv. Mater.* **2008**, *20*, 2556.

[78] S. E. Shaheen, C. J. Brabec, N. S. Sariciftci, F. Padinger, T. Fromherz, J. C. Hummelen, *Appl. Phys. Lett.* **2001**, *78*, 841.

[79] T. Martens, J. D'Haen, T. Munters, Z. Beelen, L. Goris, J. Manca, M. D'Olieslaeger, D. Vanderzande, L. De Schepper, R. Andriessen, *Synt. Metals* **2003**, *138*, 243.

[80] H. Hoppe, M. Niggemann, C. Winder, J: Kraut, R. Hiesgen, A. Hinsch, D. Meissner, N. S. Sariciftci, *Adv. Funct. Mater.* **2004**, *14*, 1005.

[81] F. Zhang, K. G. Jespersen, C. Bjoerstroem, M. Svensson, M. R. Andersson, V. Sundström, K. Magnusson, E. Moons, A. Yartsev, O. Inganäs, *Adv. Funct. Mater.* **2006**, *16*, 667.

[82] Q.-D. Dao, T. Hori, K. Fukumura, T. Masuda, T. Kamikado, A. Fujii, Y. Shimizu, M. Ozaki, *Organic Electron.* **2013**, *14*, 2628.

[83] M. Pfaff, M. F. G. Klein, E. Müller, P. Müller, A. Colsmann, U. Lemmer, D. Gerthsen, *Micros. Microanal.* **2012**, *18*, 1380.

[84] H.-Y. Chen, J.-L. Wu, C.-T. Chen, C.-T. Chen, *Chem. Commun.* **2012**, *48*, 1012.

[85] J. M. Kroon, M. M. Wienk, W. J. H. Verhees, J. C. Hummelen, *Thin Solid Films* **2002**, *403*, 223.

[86] G. Li, V. Shrotriya, J. Huang, Y. Yao, T. Moriarty, K. Emery, Y. Yang, *Nature Mater.* **2005**, *4*, 864.

[87] Y. Liang, Z. Xu, J. Xia, S.-T. Tsai, Y. Wu, G. Li, C. Ray, L. Yu, *Adv. Mater.* **2010**, *22*, E135.

[88] H. K. Gummel, *IEEE Trans. Electron Devices,* **1964**, *11*, 455.

[89] H. T. Nicolai, G. A. H. Wetzelaer, M. Kuik, A. J. Kronemeijer, B. De Boer, P. W. M. Blom, *Appl. Phys. Lett.* **2010**, *96*, 172107.

[90] L. J. A. Koster, E. C. P. Smits, V. D. Mihailetchi, P. W. M. Blom, *Phys. Rev. B* **2005**, *72*, 085205.

[91] M. Kuik, L. J. A. Koster, A. G. Dijkstra, G. A. H. Wetzelaer, P. W. M. Blom, *Organic Electron.* **2012**, *13*, 969.

[92] L. J. A. Koster, O. Stenzel, S. Oosterhout, M. M. Wienk, V. Schmidt, R. A. J. Janssen, *Adv. Energy Mater* **2013**, *3*, 615.

[93] C. Groves, R. G. E. Kimber, A. B. Walker, *J. Chem. Phys.* **2010**, *133*, 144110.

[94] S. Selberherr, *Analysis and simulation of semiconductor devices*. Springer Science & Business Media, Wien, 2012.

[95] A. Einstein, *Annalen der physik* **1905**, *4*, 549.

[96] Y. Roichman, N. Tessler, *Appl. Phys. Lett.* **2002**, *80*, 1948.

[97] G. A. H. Wetzelaer, L. J. A. Koster, P. W. M. Blom, *Phys. Rev. Lett.* **2011**, *107*, 066605.

[98] J. D. Kotlarski, P. W. M. Blom, L. J. A. Koster, M. Lenes, L. H. Slooff, *J. Appl. Phys.* **2008**, *103*, 084502.

[99] V. S. Gevaerts, L. J. A. Koster, M. M. Wienk, R. A. J. Janssen, *ACS Appl. Mater. Interfaces* **2011**, *3*, 3252.